doi:10.1016/j.jmb.2006.10.008 J. Mol. Biol. (2007) 365, 590–602

JMB

Available online at www.sciencedirect.com

ScienceDirect

ELSEVIER

Mechanism of Template-independent Nucleotide Incorporation Catalyzed by a Template-dependent DNA Polymerase

Kevin A. Fiala[1,2], Jessica A. Brown[1,2], Hong Ling[3], Ajay K. Kshetry[4] Jun Zhang[1], John-Stephen Taylor[4], Wei Yang[5] and Zucai Suo[1,2]*

[1]*Department of Biochemistry The Ohio State University Columbus, OH 43210, USA*

[2]*The Ohio State Biochemistry Program, The Ohio State University, Columbus OH 43210, USA*

[3]*Department of Biochemistry University of Western Ontario London, Ontario Canada N6A 5C1*

[4]*Department of Chemistry Washington University St. Louis, MO 63130, USA*

[5]*Laboratory of Molecular Biology, National Institute of Diabetes and Digestive and Kidney Diseases National Institutes of Health Bethesda, MD 20892, USA*

**Corresponding author*

Numerous template-dependent DNA polymerases are capable of catalyzing template-independent nucleotide additions onto blunt-end DNA. Such non-canonical activity has been hypothesized to increase the genomic hypermutability of retroviruses including human immunodeficiency viruses. Here, we employed pre-steady state kinetics and X-ray crystallography to establish a mechanism for blunt-end additions catalyzed by *Sulfolobus solfataricus* Dpo4. Our kinetic studies indicated that the first blunt-end dATP incorporation was 80-fold more efficient than the second, and among natural deoxynucleotides, dATP was the preferred substrate due to its stronger intrahelical base-stacking ability. Such base-stacking contributions are supported by the 41-fold higher ground-state binding affinity of a nucleotide analog, pyrene nucleoside 5′-triphosphate, which lacks hydrogen bonding ability but possesses four conjugated aromatic rings. A 2.05 Å resolution structure of Dpo4•(blunt-end DNA)•ddATP revealed that the base and sugar of the incoming ddATP, respectively, stack against the 5′-base of the opposite strand and the 3′-base of the elongating strand. This unprecedented base-stacking pattern can be applied to subsequent blunt-end additions only if all incorporated dAMPs are extrahelical, leading to predominantly single non-templated dATP incorporation.

Keywords: pre-steady state kinetics; X-ray crystal structure; blunt-end addition; Dpo4; pyrene nucleoside 5′-triphosphate

Introduction

Since the discovery of *Escherichia coli* DNA polymerase I in the 1950s, six families of DNA polymerases, which participate in diverse physiological roles, have been discovered in all three domains of life. A DNA polymerase, according to its orthodoxical definition, is an enzyme that catalyzes the formation of polynucleotides in a template-dependent manner in the presence of four deoxynucleotides (dNTPs).[6] Although this ability to synthesize nucleotide polymers is affected by numerous factors including the overall mechanism, which is polymerase-specific, the selection of a correct incoming dNTP is governed by proper Watson–Crick base-pairing between the base of the dNTP and the template base opposite the incoming dNTP as well as geometric selection.[1,2] However, many archaeal, bacterial, eukaryotic, and viral DNA polymerases are also found to catalyze non-templated nucleotide additions to the 3′-termini of blunt-end DNA. These enzymes include thermostable polymerases (*Taq* DNA polymerase from *Thermus aquaticus*, *Tfi* DNA polymerase from *Thermus filiformis*, *Tth* DNA polymerase from *Thermus thermophilus*),[3] *Escherichia coli* DNA polymerase I,[4] DNA polymerase α from chick embryo,[5] rat DNA polymerase β,[5] yeast DNA polymerases I[5] and η,[6] and reverse transcriptases (RT) from avain myeloblastosis virus[5] and human immunodeficiency virus 1 (HIV-1).[7] Although the

Abbreviations used: dNTP, deoxynucleotide; BPDE, benzo[a]pyrene diol epoxide; Dpo4, *Sulfolobus solfataricus* DNA polymerase IV; HIV-1, human immunodeficiency virus type-1; dPTP, pyrene nucleoside 5′-triphosphate.

E-mail address of the corresponding author: suo.3@osu.edu

precise biological significance of non-templated blunt-end additions has not been resolved, studies of HIV-1 RT suggest that the incorporation of additional bases before (−) strand DNA transfer contribute to the hypermutability of the HIV-1 genome.[7] Interestingly, the non-templated blunt-end nucleotide incorporations catalyzed by most of the aforementioned enzymes are dominated by a single dATP incorporation. This activity has been cleverly exploited by Promega Corporation (pGEM-T easy vector system) and Invitrogen (TOPO TA PCR cloning system) in the development of TA cloning kits. In these kits, a thermostable DNA polymerase, like *Taq* DNA polymerase, is used to generate PCR products with a 3′-protruding base A, which forms a Watson–Crick base-pair with the 5′-protruding base T of a vector to facilitate the ligation between the PCR product and vector. Surprisingly, however, the kinetic and structural bases for the non-templated blunt-end polymerization has yet to be established.

Here, we used *Sulfolobus solfataricus* DNA polymerase IV (Dpo4) as a model enzyme to investigate the mechanistic basis for non-templated blunt-end additions. *S. solfataricus* is an aerobic crenarchaeon that grows optimally at 80 °C and pH 2–4.[8] Dpo4, a model lesion bypass polymerase from the Y-family, has been well characterized kinetically,[9,10] biochemically,[11–18] and structurally[14–23] in the presence of either damaged or undamged primer/template DNA substrates. The results of our pre-steady state kinetic studies demonstrated that the adenine of an incoming dATP stacked against the 5′-base of the opposite DNA strand in a blunt-end DNA substrate, leading to one predominant dATP incorporation. Using pyrene 5′-triphopshate (dPTP) as a dATP analog, we demonstrated that base stacking was the major factor to facilitate nucleotide binding. These kinetic predictions were supported by the solved crystal structure of the ternary complex of Dpo4• blunt-end DNA•ddATP.

Results

Determination of equilibrium dissociation constant of Dpo4•blunt-end DNA

To determine whether or not the binding affinity of Dpo4 to DNA was affected by the absence of an extruding 5′ template region, the gel-mobility shift assay was used to determine the equilibrium dissociation constant (K_d) of the binary complex of Dpo4 and B-1, a 5′-^{32}P-labeled blunt-end DNA substrate (Table 1). A solution containing a fixed concentration of B-1 was incubated with increasing concentrations of Dpo4 (Materials and Methods). After equilibration, the binary complex Dpo4•D-1 and free B-1 were separated using native polyacrylamide gel electrophoresis (Figure 1(a)). Notably, each B-1 molecule containing two blunt-ends was not simultaneously bound by two molecules of Dpo4. This is likely due to the limited size of B-1 (21/21-mer), which only allowed one protein molecule to bind. The binary complex concentration was calculated and plotted against Dpo4 concentration and the data were fit to equation (1) (Materials and Methods) to yield a K_d of 38(±3) nM (Figure 1(b)). In parallel, a similar gel-mobility shift assay (data not shown) was employed to measure the K_d of the binary complex of Dpo4 and D-1, a recessed primer/template DNA (Table 1). The Dpo4•D-1 complex dissociated with a K_d of 10(±2) nM. Thus, Dpo4 binds ~fourfold weaker to blunt-end DNA. To compensate for the modestly weaker binding affinity of Dpo4•blunt-end DNA, we decided to measure blunt-end nucleotide incorporation efficiency under single-turnover conditions in which the enzyme was in molar excess over DNA in order to eliminate complications from multiple enzyme turnovers.

Efficiency of nucleotide incorporation onto blunt-end DNA

Initially, we tested whether each dNTP could be incorporated onto blunt-end DNA by Dpo4. A time course of individual dNTP incorporation onto B-1 was performed and the results from sequencing gel analysis of the reactions showed that Dpo4 did incorporate each dNTP (Figure 2(a)–(d)) but with different efficiencies. In addition, each dNTP could be inefficiently incorporated a second time, however the first incorporation dominated.

To determine the preference of Dpo4 catalyzed nucleotide incorporation onto blunt-end DNA, single-turnover experiments were designed to quantify the substrate specificity or efficiency (k_p/K_d), by

Table 1. DNA substrates

B-1	5′-CGCAGCCGTCCAACCAACTCA-3′
	3′-GCGTCGGCAGGTTGGTTGAGT-5′
B-2	5′-TGAGTTGGTTGGACGGCTGCG-3′
	3′-ACTCAACCAACCTGCCGACGC-5′
B-1A	5′-CGCAGCCGTCCAACCAACTCAA-3′
	3′-GCGTCGGCAGGTTGGTTGAGT-5′
D-1	5′-CGCAGCCGTCCAACCAACTCA-3′
	3′-GCGTCGGCAGGTTGGTTGAGTAGCAGCTAGGTTACGGCAGG-5′
X-1	5′-TCT<u>A</u>GAATCCTTCCCCC-3′
	3′-CTT<u>A</u>GGAAGGGGG-5′

All DNA substrates except X-1 contained a 5′-radiolabeled top strand. The underlined/italicized <u>A</u> is a BPDE-adenine adduct.

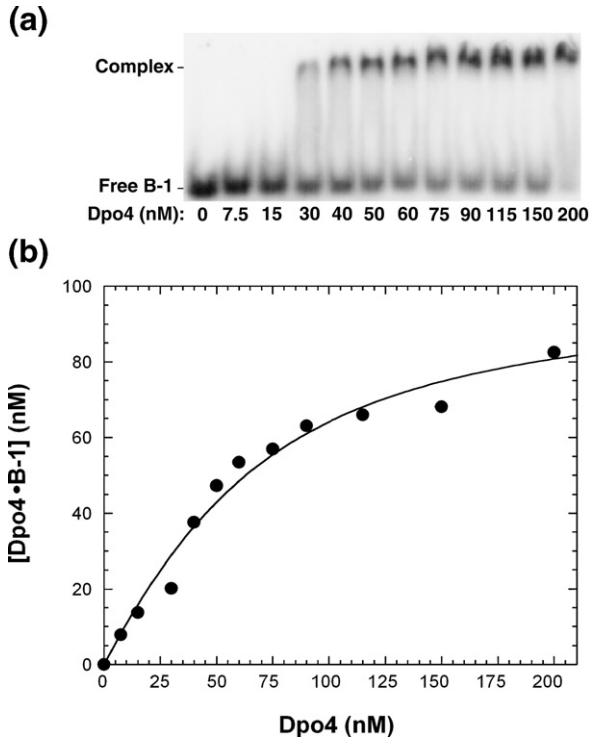

Figure 1. Gel mobility shift assay to determine Dpo4•B-1 equilibrium dissociation constant. (a) Reactions containing 100 nM 5′-[^{32}P]B-1 were incubated with increasing concentration of Dpo4 as indicated in the gel picture followed by native gel analysis to resolve binary complex from unbound B-1. (b) Binary complex formation [Dpo4•B-1] was plotted against Dpo4 concentration and the resulting data points were fit via quadratic regression (equation 3) to yield a K_d of 38±3 nM.

measurement of the maximum rate of incorporation (k_p) and equilibrium dissociation binding constant (K_d) for the incorporation of each dNTP onto B-1 (Materials and Methods). Typically, after titration of the Dpo4•B-1 binary complex with an incoming nucleotide (e.g. dATP•Mg^{2+}), the reactions were stopped by addition of EDTA, which inactivated Dpo4 by chelating its metal cofactor Mg^{2+}. The reaction mixtures were analyzed *via* denaturing gel electrophoresis. Product concentrations were plotted against reaction time and fit to equation (2) (Materials and Methods) to yield an observed incorporation rate constant (k_{obs}) at each dATP•Mg^{2+} concentration (data not shown). The k_{obs} values were then plotted against the concentration of dATP•Mg^{2+} and the data were fit to equation (3) (Materials and Methods) to yield k_p and K_d (Table 3). With B-1, dATP was incorporated with a k_p of 0.0035(±0.0003) s^{-1} and a K_d of 571(±132) μM (Figure 3(a)). The substrate specificity (k_p/K_d) was then calculated to be 6.1×10^{-6} $\mu M^{-1}s^{-1}$ (Table 3). Similar single-turnover experiments were carried out for the incorporations of dCTP, dGTP, and dTTP onto B-1 (data not shown) and the kinetic parameters were listed in Table 3. To evaluate which nucleotide was the most efficient substrate, the efficiency ratio, $(k_p/K_d)_{dNTP}/(k_p/K_d)_{dATP}$, was then calculated and was in the range of 0.02–1 (Table 3). Based on the efficiency ratios, Dpo4 selects nucleotides for blunt-end addition in the order of dATP>dTTP>dCTP>dGTP, with dATP favored by five to 50-fold over the other nucleotides. Unexpectedly, dTTP was incorporated only fivefold less efficiently than dATP, while dGTP had the smallest substrate specificity of all four incorporations. These results suggested that dATP was incorporated 79%

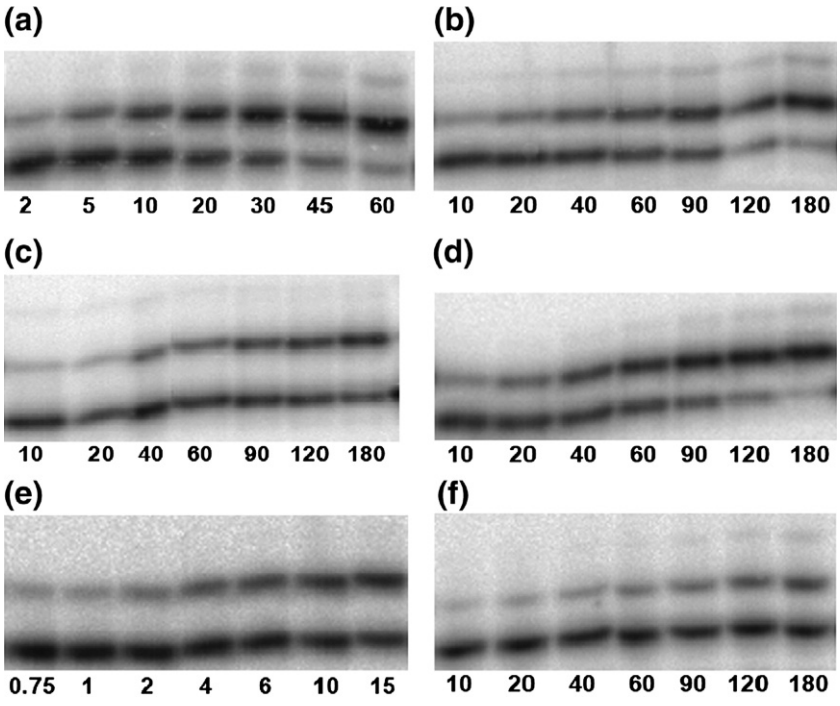

Figure 2. Series of polyacrylamide gel pictures showing time courses of product formation under the following conditions either onto B-1: (a) 200 μM dATP, (b) 1,300 μM dCTP, (c) 1,300 μM dGTP, (d) 400 μM dTTP, (e) 2 μM dPTP, or onto the B-1A substrate, (f) 1,300 μM dATP. Remaining primer, 21-mer in (a)–(e), 22-mer in (f), is shown at the bottom of each gel image with extended products located sequentially above it. Reaction time (minutes) is denoted below the corresponding lane.

Table 2. Summary of X-ray crystallographic data

Space group	$P2_12_12$
Unit cell (*a,b,c)* (Å)	98.1, 101.9, 52.4
No. of complex in AU	1
Non-hydrogen atoms	3697
Resolution range (Å)[a]	26.7–2.05 (2.09–2.05)
R_{merge}[a,b]	0.063 (0.340)
Unique reflection	31,879
Completeness (%)[a]	97.5 (93.7)
R-value[c]	0.230
R_{free}[d]	0.284 (954 reflections)
r.m.s.d. bond length (Å)	0.011
r.m.s.d. bond angle (°)	1.30
Ave. *B*-value (Wilson) (Å^2)	45.3 (47.3)

[a] Data completeness in the highest resolution shell is shown in parenthesis.
[b] $R_{merge} = \sum_h \sum_i | I_{hi} - \langle I_h \rangle | / \sum \langle I_h \rangle$, where I_{hi} is the intensity of the *i*th observation of reflection *h*, and $\langle I_h \rangle$ is the average intensity of redundant measurements of the *h* reflections.
[c] $R\text{-value} = \sum | | F_o | - | F_c | | / \sum | F_o |$, where F_o and F_c are the observed and calculated structure-factor amplitudes.
[d] R_{free} is monitored with the reflections excluded from refinement in parenthesis.

of the time onto B-1 compared to 16%, 3%, and 2% for dTTP, dCTP, and dGTP, respectively. Interestingly, the substrate specificity for blunt-end dATP incorporation (6.1×10^{-6} $\mu M^{-1}s^{-1}$) was almost identical to the incorporation efficiency of a mismatched dATP (9.9×10^{-6} $\mu M^{-1}s^{-1}$, Table 3) into a recessed primer/template D-1 (Table 1). Moreover, the K_d and k_p values for the blunt-end dATP incorporation (Table 3) were also similar to the corresponding values of the mismatched dATP incorporation. Thus, the blunt-end dATP incorporation was kinetically indistinguishable from the "template directed" incorrect dATP incorporation.

However, the DNA sequence of the B-1 substrate facilitated the possibility of an incoming dATP forming a Watson–Crick base-pair with the 5′-T of the opposite strand, thus promoting its incorporation if the terminal base-pair between the 5′-T and the 3′-A of the elongating strand "melted". To examine this hypothesis, we measured the nucleotide incorporation efficiency with another blunt-end DNA substrate B-2 (Table 1) under identical single-turnover conditions. Notably, B-1 and B-2 are identical in sequence context, yet differ with respect to which oligonucleotide strand is 5′-radiolabeled. The kinetic results with B-2 (Table 3) demonstrated that Dpo4 had the same nucleotide selection hierarchy as B-1, and thus, incorporation of dATP onto B-2 was favored over all other nucleotide incorporations by a kinetically similar ten to 33-fold. The incorporation probabilities onto B-2 were calculated to be 81%, 8%, 8%, and 2% for dATP, dTTP, dCTP, and dGTP, respectively. Moreover, the incorporation efficiency of dGTP, which was notably the lowest among all four dNTPs onto B-2 (Table 1), strongly invalidated any hypothesized influence from terminal base-pair melting to blunt-end additions catalyzed by Dpo4.

Efficiency of pyrene nucleoside 5′-triphosphate incorporation onto blunt-end and recessed DNA

Watson–Crick base-pairing between an incoming nucleotide and a template base observed with recessed primer/template DNA was shown to be irrelevant for nucleotide selection by Dpo4 when it catalyzed blunt-end additions. The kinetic preference for dATP incorporation onto both B-1 and B-2 was thus likely due to its favorable base-stacking with the 3′-terminal base of the elongating strand. To test this hypothesis we measured the incorporation efficiency of pyrene nucleoside 5′-triphosphate

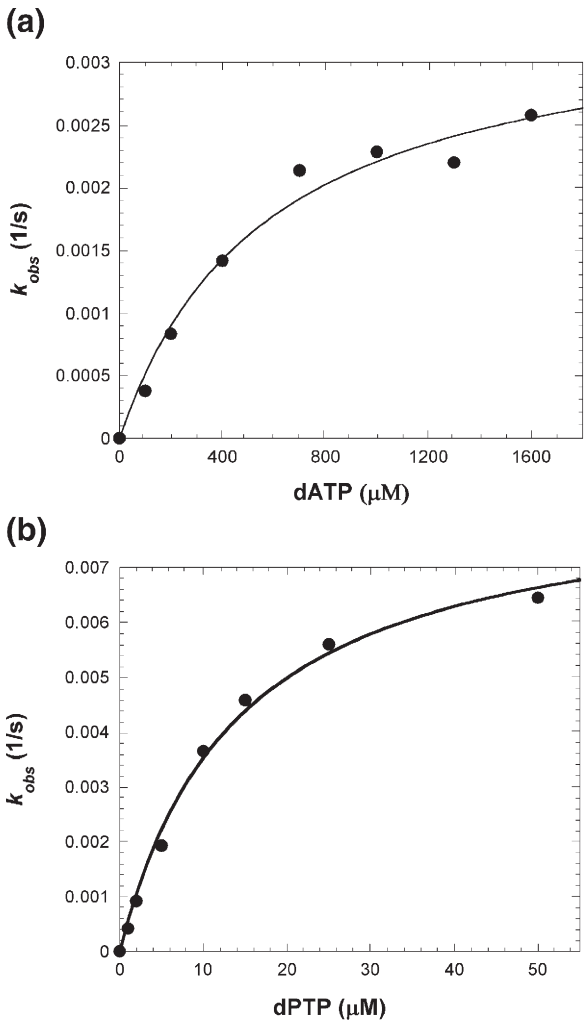

Figure 3. Concentration dependence on the rate of dATP and dPTP incorporation onto B-1. A preincubated solution of Dpo4 (120 nM) and 5′-[^{32}P]B-1 (30 nM) was mixed with an increasing concentration of dNTP•Mg^{2+} for various times. The individual reactions were then quenched by 0.37 M EDTA. (a) The single exponential rates for each individual time course were plotted as a function of dATP concentration. The rate data were then fit to the hyperbolic equation (equation 2) yielding a k_p of 0.0035(±0.0003) s^{-1} and a K_d of 571(±132) μM. (b) Likewise, the dependence of dPTP concentration on the single-turnover rate onto B-1 was plotted, as above, to yield a k_p of 0.0085(±0.0004) s^{-1} and a K_d of 14(±2) μM.

(dPTP, Scheme 1), a dNTP analog, onto B-1. dPTP was chosen as a probe because its large non-polar base precludes hydrogen bonding with any natural bases, while possessing superior aromatic π-stacking capabilities relative to dATP.[24,25] Figure 2(e) shows that Dpo4 only incorporated dPTP onto B-1 once. Using the same single-turnover assay described above, we then determined a k_p of 8.5 (±0.4) × 10^{-3} s^{-1} and strikingly, a low K_d of 14(±2) μM (Figure 3(b)) for the incorporation of dPTP onto B-1 (Table 3). The incorporation efficiency of dPTP incorporation onto B-1 was calculated to be 6.1×10^{-4} $\mu M^{-1}s^{-1}$, which was 100-fold higher than dATP incorporation efficiency (Table 3).

To examine whether or not the dramatic kinetic difference between the incorporations of dPTP and dATP was affected by a template base, we determined the pre-steady state kinetic parameters for dPTP incorporation into D-1, a recessed primer/template DNA substrate (Table 1), and listed the kinetic parameters in Table 3. Overall, dPTP bound 20-fold tighter, was incorporated 9.5-fold faster, and possessed 200-fold higher incorporation efficiency than mismatched dATP into D-1 (Table 3). In contrast, dPTP was incorporated 21-fold less efficiently than a matched dTTP into D-1 although it possessed eightfold higher ground-state binding affinity. The reason for the decreased efficiency was due to a 165-fold slower rate constant for dPTP incorporation into D-1 (Table 3).

Efficiency of the second nucleotide incorporation onto blunt-end DNA

(Figure 2(a)–(d) suggests that Dpo4, like other DNA polymerases, was inefficient at catalyzing the second nucleotide incorporation onto blunt-end DNA. To confirm this observation, similar single-turnover experiments were performed (see above) to determine the incorporation efficiency onto B-1A (Table 1). B-1A contained a 3′-overhang dAMP and represented the DNA product after Dpo4 "incorporated" the preferred nucleotide onto B-1. Single nucleotide incorporation assays with dCTP, dGTP, and dTTP only showed trace product formation onto B-1A even after 2 h and were thereby considered kinetically irrelevant (data not shown). However, we were able to observe the incorporation of dATP onto B-1A (Figure 2(f)) and determined the following kinetic parameters: $k_p = 3.6 (\pm 0.2) \times 10^{-5}$ s^{-1}, $K_d = 464 (\pm 72)$ μM, and $k_p/K_d = 7.7 \times 10^{-8}$ $\mu M^{-1}s^{-1}$ (Table 3). Interestingly, the k_p/K_d value for the incorporation of dATP onto B-1A (Table 1) was 79-fold lower than the incorporation efficiency of dATP onto B-1, and was due to a 97-fold decrease in k_p, rather than a change in K_d. These results indicated that the second dATP incorporation was significantly less efficient than the first dATP incorporation onto blunt-end DNA.

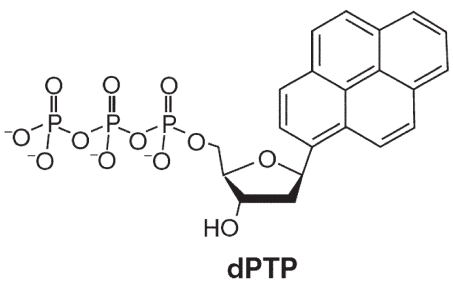

dPTP

Scheme 1.

Crystal structure of ternary complex Dpo4•blunt-end DNA•dATP

Previously, we have published two ternary crystal structures of Dpo4, dATP and a 13/16-mer DNA substrate which contained a benzo[a]pyrene diol epoxide (BPDE)-adenine adduct at the last base-pair between the template and primer strand.[21] In these structures, Dpo4 functions as a typical template-dependent DNA polymerase, binding to the primer-template junction with the incoming dATP positioned opposite the templating dT. Interestingly, when BPDE-dA adduct was placed at the templating position in X-1 (Table 1), we obtained crystals of a ternary complex, in which Dpo4 binds to the blunt-end of 13/17-mer with an incoming ddATP occupying the active site (Figure 4). This high-resolution (2.05 Å) structure showed that the single-stranded portion of the 17-mer containing the BPDE-dA adduct was fully exposed to bulk solvent and thus disordered. The overall structure of Dpo4 (residues 1–348) was similar to the previously published type I structure[19] without significant protein structural changes with the DNA substrate remaining B-type. One minor difference was that seven additional residues at the C terminus of Dpo4 were ordered and formed a flexible loop. The striking difference was that the base of the incoming ddATP was shifted toward the center of the helical duplex due to the absence of a templating base, and its six-membered ring stacked with the 5′-terminal base (dG) of the opposite strand. As a result of the ddATP shifting, its deoxyribose interacted with the 3′-terminal base (Figure 4) in addition to its interaction with amino acid residue Y12 as observed in other Dpo4 ternary complexes.[19–22] In addition, only one divalent metal ion (Ca^{2+}) was found in the active site of Dpo4. The distance between the 3′-OH (nucleophile) and the α-phosphate of ddATP was 5.71 Å, which was beyond the 3.4 Å observed for an optimum catalytically active DNA polymerase ternary complex.[26]

Discussion

Base-stacking governs blunt-end addition

Dpo4 is an archaeal Y-family DNA polymerase that can bypass a variety of DNA lesions including abasic sites, cisplatin-DNA adducts, *cis-syn* TT

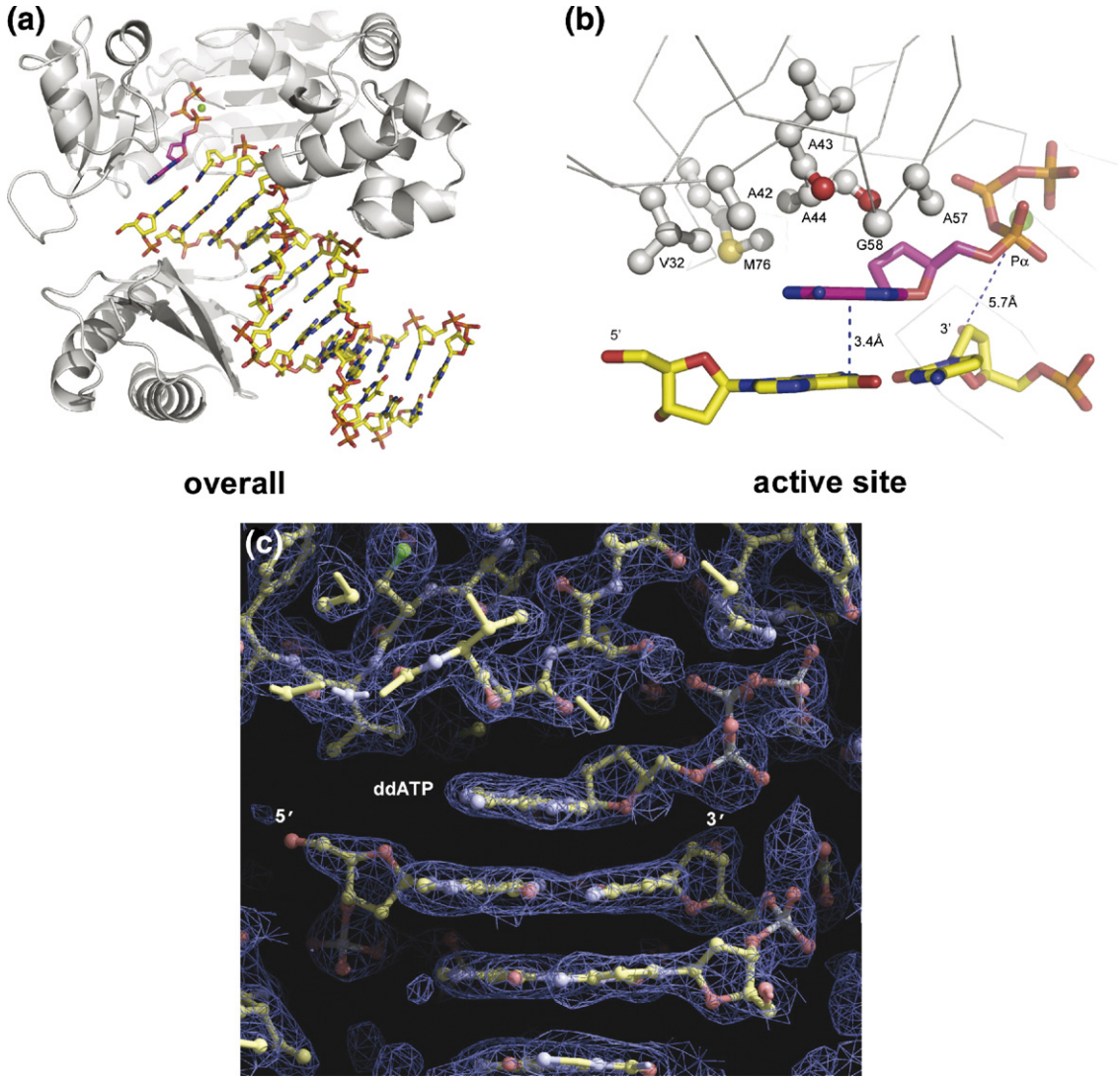

Figure 4. Crystal structure of Dpo4•blunt-end X-1•ddATP (2.05 Å). (a) Overall ternary structure. Dpo4 was shown in grey ribbons while DNA and ddATP were shown as ball-and-stick models. The ddATP is highlighted in magenta. The Ca^{2+} ion was shown in a green sphere. (b) The zoomed in view of the active site including ddATP and the blunt-end base-pair. The residues in contact with ddATP were shown as ball-and-stick models (grey for atom C, red for atom O, yellow for atom S). Only the side chain and main chain atoms involved were shown. (c) $2F_o$ - F_c electron density map contoured at 1.2 σ (light-blue) of the active site. The amino acid residues, two blunt-end DNA base-pairs, and incoming ddATP were shown as ball-and-stick models.

dimers, 6-4 TT dimers, acetyl aminofluorene-DNA adducts (AAF), and benzo[*a*]pyrene hydrocarbon adducts.[11,18,21] Since it naturally lacks proof-reading exonuclease activity, the fidelity of Dpo4 (10^{-3}–10^{-4}) with undamaged DNA at 37 °C[9] is much lower than the fidelity (10^{-7}–10^{-8}) of typical replicative DNA polymerases such as T7 phage DNA polymerase[27,28] and human mitochondrial DNA polymerase.[29,30] Both DNA lesion tolerance and low fidelity suggest that Dpo4 may possess the template-independent nucleotidyl transferase activity that has been observed with other template-dependent DNA polymerases.[3,4,5,7] This hypothesis was confirmed by the elongation of B-1 in the presence of each dNTPs·Mg^{2+} (Figure 2(a)–(d)).

The incorporation efficiency values in Table 3 confirmed that the most efficient substrate for the blunt-end addition onto both B-1 and B-2 catalyzed by Dpo4 was dATP, followed by dTTP, dCTP, and dGTP. Although B-1 and B-2 have identical DNA sequences, the nearest neighbor base-pair for blunt-end additions, A:T in B-1 and G:C in B-2, were different, indicating that the selection of dATP for Dpo4-catalyzed blunt-end additions was sequence-independent. dATP has also been found to be the most favorable nucleotide for blunt-end additions catalyzed by other template-dependent polymerases, although the selection order of the remaining dNTPs varies,[3,4,5,7] e.g. dGTP > dTTP > dCTP with HIV-1 RT.[7] Due to the lack of template information in B-1 and B-2 opposite an incoming nucleotide to form Watson–Crick base-pairs, the ground-state binding affinity of this nucleotide was likely governed by its base-stacking with the blunt-

end bases in addition to its van der Waals interactions with the active site residues of Dpo4 (A44, A57, and M76).[14,19] Previous thermodynamic studies of short DNA duplexes containing 5′-dangling ends by Guckian *et al*.[31] have determined the base-stacking free energies (kcal/mol) for the 5′-protruding base: A (1.0), G (0.7), T (0.6), and C (0.5). Other thermodynamic studies[32–34] have also revealed that adenine, regardless of 5′ or 3′-protuding, stacks better than the other three natural bases with DNA duplexes. Thus, we conclude that base-stacking plays a major role in the selection of dATP by Dpo4 and other DNA polymerases for template-independent blunt-end additions. This conclusion was substantiated by the 41-fold higher ground-state binding affinity of the nucleotide analog dPTP (Scheme 1) to Dpo4•B-1 than dATP (Table 3) as well as the strong correlation between the order of base stacking energies (dPTP>dATP>dGTP>dTTP>dCTP) and the k_p, K_d, and k_p/K_d with the exception of dGTP. The measured blunt-end base-stacking free energy of the pyrene base (1.7 kcal/mol) is significantly higher than adenine (1.0 kcal/mol).[31] The stronger stacking of dPTP, due to its four conjugated benzene rings (Scheme 1), over dATP with the terminal base(s) of B-1 significantly lowered the K_d for the blunt-end incorporation of dPTP. In addition, we speculate that the increased stacking energies of each successive dNTP lead to a faster turnover rate constant (k_p) due to the inherent tighter binding of the particular dNTP in the ground-state that increases the probability of incorporation.

Base-stacking controls K_d while Watson–Crick hydrogen bonding governs k_p

Strikingly, the strong stacking of dPTP also facilitated its binding to the binary complex of Dpo4 and recessed D-1 (Table 1). dPTP bound to Dpo4•D-1 in the ground-state with eight and 20-fold higher affinity than matched dTTP and mismatched dATP, respectively (Table 3). The binding of dTTP likely involved Watson–Crick hydrogen bonds with the template base A, yet it was only about twofold tighter than the binding of mismatched dATP. The difference in the binding affinity of dPTP and dTTP further suggested that base-stacking was more critical to the ground-state binding affinity of an incoming nucleotide than hydrogen-bonding. In contrast, dPTP incorporation into D-1 was only slightly faster than typical mismatched dNTPs, but was 165-fold slower than the incorporation of matched dTTP into Dpo4•D-1. Thus, the Watson–Crick hydrogen bonds formed between an incoming nucleotide and a template base have a larger influence on the maximum incorporation rate constant k_p than base-stacking. This conclusion was supported by the fact that mismatched and matched dNTPs, which only differ in Watson–Crick hydrogen bonds, are incorporated with a larger difference in k_p (100 to 1000-fold) than in K_d (one to 100-fold) for all kinetically characterized DNA polymerases.[9] The reason for this is due to the proper spatial orientation of the incoming dNTP with respect to the DNA 3′-OH guided by the Watson–Crick hydrogen bonds in a matched base-pair. The tight binding of a nucleotide at a polymerase active site due to strong base-stacking interactions may not perfectly position this nucleotide for catalysis because it requires subtle adjustments by the Watson–Crick hydrogen bonds. However, both Watson–Crick hydrogen bonding and base-stacking mathematically contribute to the incorporation efficiency (k_p/K_d) of a DNA polymerase. There are many examples to support this general conclusion and importantly, one of these two parameters (k_p or K_d) may have a larger influence on the substrate specificity than the other. With respect to the importance of hydrogen bonds, difluorotoluene nucleoside 5′-triphosphate, a nucleotide analog that cannot form Watson–Crick hydrogen bonds but has similar size, shape, and conformation as dTTP, is incorporated opposite a template base A with 220-fold and 10^6-fold lower substrate specificity than dTTP catalyzed by yeast DNA polymerase η[35] and human DNA polymerase κ,[36] respectively. However, as shown in Table 3, matched dTTP was incorporated 20-fold more efficiently than dPTP into D-1, suggesting that the Watson–Crick hydrogen bonds in the base-pair dTTP:A contribute more significantly than the base-stacking interactions in the base-pair dPTP:A to the efficiency of nucleotide incorporation catalyzed by Dpo4. The importance of hydrogen bonding shown here is similar to what has been revealed for incorporation catalyzed by human DNA polymerase β (X-Family polymerase) yet differs significantly from the lack of importance of hydrogen bonds for incorporation catalyzed by the A-Family DNA polymerase T7 phage DNA polymerase.[37] Additionally, the fact that dPTP was more efficiently incorporated into D-1 than mismatched dNTPs indicated that the large base of dPTP (surface area, 217 Å^2)[31] did not perturb its incorporation efficiency and the active site of Dpo4 is flexible and/or spacious. Thus, both hydrogen bonding and base-stacking contribute disproportionally based on the specific catalyzed reaction.

Mechanism of blunt-end additions

The above discussion demonstrated that a polymerase selected dATP for blunt-end additions due to superior stacking with the terminal bases. What is the nature of dATP stacking? The ternary structure in Figure 4 showed that the six-membered aromatic ring of the base of ddATP surprisingly stacked against the six-membered aromatic ring of the 5′-G of the opposite strand while the sugar of ddATP stacked and possessed hydrophobic interactions with the 3′-terminal base C of the strand that will be extended. The vertical distance between the base planes of ddATP and 5′-G (3.4 Å) is equal to the average rise per base-pair in *B*-type DNA, suggesting that the base-stacking interactions were intense. However, in the case of dPTP incorporation, because

the base of dPTP is so large, it likely base-stacked with both 3′-A and 5′-T of B-1 simultaneously, thus significantly increasing its binding affinity. The presence of an opposing template base (D-1) will likely limit the base-stacking of dPTP to the 3′-A only, possibly accounting for the observed twofold lower affinity with D-1 than with B-1 (Table 3). Thermodynamically, the base-stacking energy difference (0.7 kcal/mol) between 5′-dangling bases pyrene (1.7 kcal/mol) and adenine (1.0 kcal/mol) in a DNA duplex was not large enough to explain the binding free energy differences, $\Delta\Delta G = -RT\ln(K_{dPTP}/K_{d,dATP})$, between dPTP and dATP with both B-1 (2.3 kcal/mol) and D-1 (1.8 kcal/mol). This indicated that other sources contributed to the higher stabilization of dPTP binding. One such source was favorable van der Waals interactions between pyrene and the active site residues (Ala43, Ala44, Ala57, Ala58, and Met76) of Dpo4.[14,19] The ternary structure in Figure 4 suggested that this possibility was likely due to the large size of pyrene, which is comparable to the total size of a canonical base-pair.[24] In addition, Figure 2(e) shows only one dPTP incorporation event. This was not surprising considering that consecutive dPTP incorporations into recessed DNA have yet to be observed in any DNA polymerase, e.g. yeast DNA polymerase η.[6] This might be due to the lack of minor groove contacts between incorporated dPMP and polymerase active site residues,[38] or more likely, due to the formation of a tightly bound dead-end ternary complex resulting from exceptional stacking of two consecutive pyrene bases (Figure 5(a)). In addition, it is plausible that if the mechanism of blunt-end addition for the second dNTP incorporation strictly follows the "base-flipped" mechanism as illustrated in Figure 5(b), the exceptional base stacking ability of the first incorporated dPMP would inhibit base-flipping and thus a second consecutive incorporation of dPTP.

For the second dATP incorporation onto B-1, Table 3 showed that the K_d value was very similar to the ground-state nucleotide binding affinity for the first dATP blunt-end addition. This indicated that a similar base-stacking pattern as observed for the first dATP possibly stabilized the binding of the second dATP. In order to maintain such a stacking scheme between the second dATP and the blunt-end base-pair, the first incorporated adenine on the 3′-terminus of the elongating strand must become extrahelical to make the terminal blunt-end base-pair accessible. The base-flipping phenomenon has been observed previously in the ternary structures of truncated human DNA polymerase λ[39] and Dpo4 (Ab-4B).[22] Consequently, the 3′-OH of the extrahelical unpaired 3′-A will be improperly positioned for efficient in-line nucleophilic attack of the α-

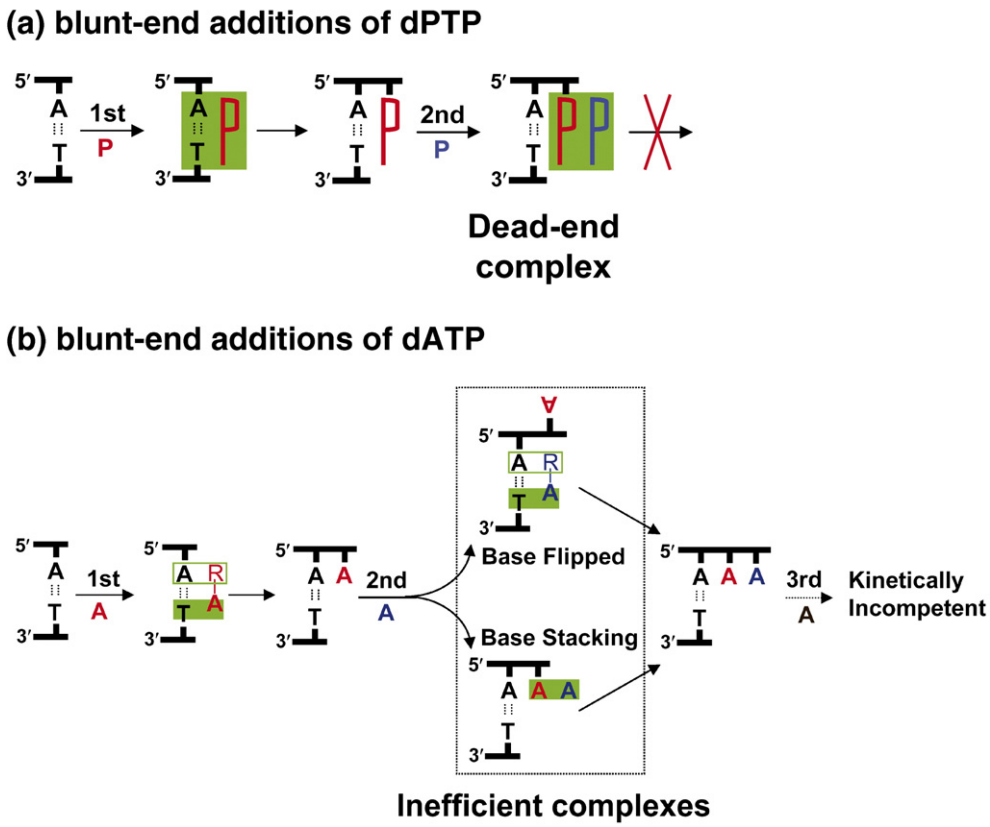

Figure 5. Proposed mechanisms of blunt-end additions of (a) dPTP and (b) dATP. dATP and dPTP are represented by **A** and **P** in different colors, respectively. The Watson-Crick hydrogen bonds were drawn as dashed lines while the base-stacking interactions were shadowed in green. The stacking interactions between the 2′-deoxyribose (R) of an incoming nucleotide and the 5′-terminal base A are displayed in a green box. The van der Waals interactions between an incoming nucleotide and Dpo4 active site residues were not shown for clarity.

phosphate of the incoming dNTP. This hypothesis is consistent with the very low k_p value for dATP incorporation onto B-1A, which was 97-fold slower than the incorporation of dATP onto B-1 (Table 3), and the dominant first blunt-end addition of a single dNTP (Figure 2). For subsequent additions after the second blunt-end dATP incorporation, more difficult active site adjustments of the DNA substrate were likely required, either precluding or rendering these incorporations extremely rare (Figure 2). Yet, one cannot rule out the possibility that the second incoming dATP simply stacked with the 3′-A without generation of an extrahelical nucleotide. This was due to similar K_d values for the incorporation of dATP onto the blunt-end substrates (B-1 and B-2), the recessed substrate (D-1), and the 3′-protruding substrate (B-1A), which overall only differ from each other by 1.3-fold. Although the ground-state binding was not significantly perturbed, the lack of template information to help orient subsequent incoming nucleotides coupled with competition between these two such mechanisms may lead to the slow observed turnover.

However, the mechanisms in Figure 5 do not unambiguously explain the slow rate constants of blunt-end additions. Table 3 has shown that the k_p values for the blunt-end incorporation of dATP and dPTP are two to three orders of magnitude slower than those of matched incorporations into D-1. This may be due to the distance between the 3′-OH of the elongating blunt-end DNA substrate and the α-phosphate of the nucleotide (5.71 Å, Figure 4), which is longer than the distance (3.4 Å) observed for correct template-dependent nucleotide incorporation.[26] With a recessed DNA substrate, our previous kinetic studies have concluded that the chemistry step is rate-limiting for incorrect nucleotide incorporation while the protein conformational change limits correct nucleotide incorporation.[10] Thus, it is plausible that blunt-end additions, like misincorporations into recessed DNA, are also limited by phosphodiester bond formation. However, our kinetic and structural data cannot exclude the possibility that a local structural rearrangement at the Dpo4 active site to reorient the bound incoming nucleotide with respect to the blunt-end DNA, especially after the binding of the second metal ion, could limit blunt-end additions.

Ternary crystal structure of blunt-end complex

The crystal structure showed that the incoming ddATP was mainly stabilized by aromatic stacking. However, instead of stacking with the elongating strand, the incoming ddATP was shifted toward the center of the DNA helix by ~2 Å when compared to the position of ddADP in the type I complex[19] (Figure 6). In this configuration, the adenine of ddATP was extensively stacked against the 5′-terminal base of the opposite strand while its deoxyribose made van der Waals interactions with the same strand 3′-terminal base. In addition, the stubby finger domain of Dpo4 established very few van der Waals contacts with ddATP, which were between the adenine and the small hydrophobic residues A44, A57, M76, and the main chain atoms of A43 and G58 (Figure 4). The interactions with A43 and G58 were not observed in Figure 6(a), due to the inward movement of the incoming nucleotide in Figure 6(b). The enhanced stacking and van der Waals interactions compensated for the lack of Watson–Crick base-pairing and accounted for the similar K_d with blunt-end B-1 and the recessed D-1 (Table 3). However, the significant decrease in the k_p was most likely due to the lack of Watson–Crick hydrogen bonds that would normally help properly orient the incoming nucleotide in the active site of Dpo4 for catalysis. This effect on k_p can be seen with each subsequent incorporation onto B-1 (Table 3). Clearly the optimized stacking of ddATP with blunt-end DNA was achieved at the expense of misalignment of DNA, dNTP, and metal ions in

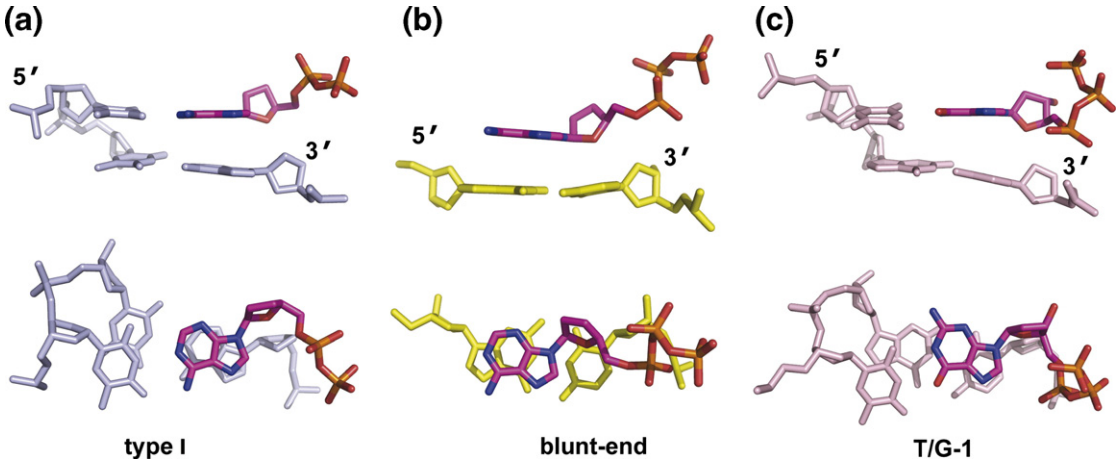

Figure 6. Comparison of the incoming nucleotide (magenta) positions in the active sites of three different Dpo4 ternary structures. The nucleotides were shown in the side (upper panel) and top (lower panel) views. (a) Type I (ddADP:T)[19]; (b) Blunt-end (ddATP:DNA); and (c) Mismatched T/G-1 (dGTP:T)[14].

the active site, leading to a greatly reduced k_p. In fact, one would imagine that the conformation trapped in the crystal structure, which we assume to be the minimal energy state, was not suitable for the nucleotide incorporation. This is most likely the reason for the lack of additional dNTP and dPTP incorporation.

In the ternary structure with a T/G mismatch in the Dpo4 active site,[14] the incoming nucleotide dGTP shifts towards the minor groove of the DNA duplex while the template base T wobbles towards the major groove due to lack of Watson–Crick hydrogen bonding (Figure 6(c)). The shifting in T/G mismatch is thus different from the center-inward movement observed in Figure 6(b) and the dGTP does not stack with the template base. This shifting led to extremely slow misincorporation, even in the case of the wobble base-pair dGTP:T[7]. In comparison, a similar center-inward movement was observed previously with Dpo4 and a DNA substrate containing an abasic site.[22] Here, the primer strand, containing a 3′-terminal dAMP, tilted toward the gap in the template strand left by the abasic lesion, yet the 3′-OH was still within 5 Å of the α-phosphate of the incoming nucleotide.[22] This structure and Figure 6(c) are clearly different from the unprecedented base-stacking scheme in Figure 6(b).

In summary, our kinetic and structural studies have established a mechanism for blunt-end additions catalyzed by Dpo4 and other DNA polymerases. We also revealed an unprecedented base-stacking pattern between an incoming nucleotide and the entire blunt-end base-pair that stabilized the binding of this nucleotide. Our results should encourage and facilitate the investigation of any evolutionary advantage for retroviruses caused by the blunt-end addition activity of their reverse transcriptases.

Materials and Methods

DNA substrates

All DNA oligonucleotides except those in X-1 (Table 1) were purchased from Integrated DNA Technologies and were purified by denaturing polyacrylamide gel electrophoresis. Their concentrations were determined by UV spectroscopy with calculated extinction coefficients. The elongating DNA strands were 5′-radiolabeled using Optikinase (USB) and [γ-^{32}P]ATP (GE Healthcare) and annealed as described.[9] The DNA substrate X-1 containing a BPDE-adenine adduct was synthesized and prepared as described.[21]

Pyrene nucleoside 5′-triphosphate

dPTP was prepared from β-pyrene nucleoside[25] as described[24] with a slight modification. Following purification on a DEAE-cellulose column and prior to conversion to the sodium salt, the triphosphate was further purified by HPLC on a Thermo Hypersil AQUACI L C18 column (4.6 mm × 250 mm, 5 μM particle size) using a 25 min linear gradient of 1.6–36.6% acetonitrile in 0.1 M triethylammonium bicarbonate (TEAB) at a flow rate of 1 ml/min with the triphosphate eluting at 20 min. The purity and identity of the sodium salt of the triphosphate was confirmed by ^{31}P NMR in $^{2}H_2O$ containing Tris-HCl (pH 7.5, 50 mM) and EDTA (2 mM): δ 22 (t), 10.6 (d), 7.6 (d). The concentration of dPTP was determined by UV spectroscopy with a molar extinction coefficient of 33,390 $M^{-1}cm^{-1}$.

Table 3. Comparison of nucleotide incorporation efficiencies for blunt-end DNA (B-1 and B-2) and recessed primer/template DNA (D-1)

dNTP	K_d (μM)	k_p (s^{-1})	k_p/K_d ($\mu M^{-1}s^{-1}$)	Efficiency ratio[a]
Incorporation onto B-1				
dATP	571±132	0.0035±0.0003	6.1×10^{-6}	1
dCTP	1581±344	0.00042±0.00005	2.7×10^{-7}	0.04
dGTP	1983±508	0.00026±0.00004	1.3×10^{-7}	0.02
dTTP	506±85	0.00062±0.00004	1.2×10^{-6}	0.20
dPTP	14±2	0.0085±0.0004	6.1×10^{-4}	100
Incorporation onto B-2				
dATP	462±98	0.0062±0.0005	1.4×10^{-5}	1
dCTP	744±344	0.0009±0.0001	1.3×10^{-6}	0.10
dGTP	894±134	0.00031±0.00002	3.5×10^{-7}	0.03
dTTP	835±142	0.0011±0.0001	1.4×10^{-6}	0.10
Incorporation onto B-1A				
dATP	464±72	$(3.6\pm0.2)\times10^{-5}$	7.7×10^{-8}	
Incorporation into D-1				
dATP[b]	578±188	0.006±0.001	9.9×10^{-6}	2.4×10^{-4}
dCTP[b]	1036±95	0.013±0.001	1.3×10^{-5}	3.1×10^{-4}
dGTP[b]	1150±312	0.007±0.001	6.0×10^{-6}	1.5×10^{-4}
dTTP[b]	230±17	9.4±0.3	4.1×10^{-2}	1
dPTP	29±3	0.057±0.003	2.0×10^{-3}	0.048

[a] Efficiency ratio = $(k_p/K_d)_{dNTP}/(k_p/K_d)_{dATP}$ with B-1 and B-2 or $(k_p/K_d)_{dNTP}/(k_p/K_d)_{dTTP}$ with D-1.
[b] Data are from Fiala & Suo.[9]

Reaction buffer R

Buffer R contains the following components optimized previously[9]: 50 mM Hepes-NaOH (pH 7.5 at 37 °C), 5 mM $MgCl_2$, 50 mM NaCl, 5 mM DTT, 10% (v/v) glycerol, 0.1 mM EDTA, and 0.1 mg/ml BSA. All concentrations reported here refer to the concentration of components after mixing. All reactions, unless otherwise noted, were carried out at 37 °C.

Measurement of the k_p and K_d for nucleotide incorporation

A pre-incubated solution containing Dpo4 (120 nM) and DNA (30 nM) in buffer R was mixed with an increasing concentration of dNTP•Mg^{2+}. Reactions were terminated at various times by the addition of 0.37 M EDTA. Product was separated from remaining substrate *via* sequencing gel electrophoresis (17% (w/v) acrylamide, 8 M urea) and quantified using a Phosphorimager 445 SI (Molecular Dynamics). The time-course of product formation was fit to equation (1) by non-linear regression using Kaleidagraph (Synergy Software) for each concentration of dNTP•Mg^{2+} to yield an observed rate constant (k_{obs}). A represents the reaction amplitude. The abstracted values for k_{obs} were then plotted as a function of the concentration of dNTP•Mg^{2+} and fit using equation (2) to give the k_p and K_d. The substrate specificity (k_p/K_d) of this nucleotide incorporation was then calculated:

$$[\text{Product}] = A[1 - \exp(-k_{obs}t)] \quad (1)$$

$$k_{obs} = k_p[\text{dNTP}]/[\text{dNTP}] + K_d \quad (2)$$

Gel mobility shift assay

The K_d for the Dpo4•DNA binary complex was determined by titrating Dpo4 (7.5–200 nM) into a solution containing 5′- [^{32}P]DNA (100 nM) in buffer T, which is identical to buffer R except its pH was 7.5 at 23 °C. After equilibrating for 15 min at 23 °C, the binary complex was then separated from free DNA using a 4.5% native polyacrylamide gel. The gel was dried and then quantified with a PhosphorImager 445. The concentration of binary complex (Dpo4•DNA) formation was plotted against the concentration of Dpo4 and fit to equation (3) to yield the K_d value. E_0 and D_0 represent the active enzyme and total DNA concentrations, respectively:

$$[\text{E•DNA}] = 1/2(K_d + E_0 + D_0) - 1/2[(K_d + E_0 + D_0)^2 - 4E_0D_0]^{1/2} \quad (3)$$

Crystallization and structure determination of a blunt-end DNA ternary complex

Wild-type Dpo4 was overexpressed and purified as described.[19] Dpo4 and X-1 (Table 1) were mixed at a 1:1.2 molar ratio with the final protein concentration of 8 mg/ml in the buffer of 20 mM Hepes (pH 7.0), 0.1 mM EDTA, 1 mM DTT, 100 mM NaCl. With the addition of 1 mM ddATP, crystals were produced by the hanging-drop method at 20 °C by using a precipitant solution of 100 mM Hepes (pH 7.0), 100 mM calcium acetate, 12% (w/v) polyethylene glycol (PEG) 3350, 2% glycerol. Crystals were transferred to a cryoprotectant solution containing the mother liquor with 25% PEG 3350 and 15% ethylene glycol and flash frozen in liquid nitrogen. Diffraction data were collected at −178 °C using a R axis IPII image plate mounted on an Rigaku RU 200 generator and processed by HKL.[40] The structures were solved by molecular replacement with CNS[41] using the type I structure as a search model.[19] The structure was iteratively adjusted with O[42] and refined using CNS and Refmac5[43,44] with all residues in the allowed regions of the Ramachandran plot (Table 2).

Protein Data Bank accession codes

The coordinates and structural factors of the ternary complex Dpo4•blunt-end X-1•ddATP have been deposited in the RCSB Protein Data Bank (accession code 2IMW).

Acknowledgements

We thank Drs J. Sayer, H. Yagi, and D. Jerina at NIH for the synthesis of the X-1 substrate. This work was supported by the National Science Foundation Career Award grant to Z.S. (Grant MCB-0447899). K.A.F. was supported by the National Institutes of Health Chemistry and Biology Interface Program at the Ohio State University (Grant T32 GM08512-08) and the American Heart Association Predoctoral Fellowship (Grant 0415129B). J.A.B. was supported by the National Institutes of Health Chemistry and Biology Interface Program at the Ohio State University (Grant 5 T32 GM008512-10). H.L. was support by the Peter Lougheed/CIHR New Investigator Award (Grant PLS-69126). W.Y. was supported by NIH intramural research program. A.K. and J.-S.T. were supported by NIH CA40463.

References

1. Echols, H. & Goodman, M. F. (1991). Fidelity mechanisms in DNA replication. *Annu. Rev. Biochem.* **60**, 477–511.
2. Moran, S., Ren, R. X. & Kool, E. T. (1997). A thymidine triphosphate shape analog lacking Watson-Crick pairing ability is replicated with high sequence selectivity. *Proc. Natl Acad. Sci. USA*, **94**, 10506–10511.
3. Mezei, L. M. & Storts, D. R. (1994). Purification of PCR products. In *PCR Technology: Current Innovations* (Griffin, H. G. & Griffin, A. M., eds), pp. 13–20. CRC Press, Baton Raton,FL.
4. Clark, J. M., Joyce, C. M. & Beardsley, G. P. (1987). Novel blunt-end addition reactions catalyzed by DNA polymerase I of *Escherichia coli*. *J. Mol. Biol.* **198**, 123–127.
5. Clark, J. M. (1988). Novel non-templated nucleotide addition reactions catalyzed by procaryotic and eucaryotic DNA polymerases. *Nucl. Acids Res.* **16**, 9677–9686.
6. Hwang, H. & Taylor, J. S. (2004). Role of base stacking and sequence context in the inhibition of yeast DNA

polymerase eta by pyrene nucleotide. *Biochemistry*, **43**, 14612–14623.
7. Peliska, J. A. & Benkovic, S. J. (1992). Mechanism of DNA strand transfer reactions catalyzed by HIV-1 reverse transcriptase. *Science*, **258**, 1112–1118.
8. She, Q., Singh, R. K., Confalonieri, F., Zivanovic, Y., Allard, G., Awayez, M. J. *et al.* (2001). The complete genome of the crenarchaeon *Sulfolobus solfataricus* P2. *Proc. Natl Acad. Sci. USA*, **98**, 7835–7840.
9. Fiala, K. A. & Suo, Z. (2004). Pre-steady-state kinetic studies of the fidelity of *Sulfolobus solfataricus* P2 DNA polymerase IV. *Biochemistry*, **43**, 2106–2115.
10. Fiala, K. A. & Suo, Z. (2004). Mechanism of DNA polymerization catalyzed by *Sulfolobus solfataricus* P2 DNA polymerase IV. *Biochemistry*, **43**, 2116–2125.
11. Boudsocq, F., Iwai, S., Hanaoka, F. & Woodgate, R. (2001). *Sulfolobus solfataricus* P2 DNA polymerase IV (Dpo4): an archaeal DinB-like DNA polymerase with lesion-bypass properties akin to eukaryotic poleta. *Nucl. Acids Res.* **29**, 4607–4616.
12. Boudsocq, F., Kokoska, R. J., Plosky, B. S., Vaisman, A., Ling, H., Kunkel, T. A. *et al.* (2004). Investigating the role of the little finger domain of Y-family DNA polymerases in low-fidelity synthesis and translesion replication. *J. Biol. Chem.* **279**, 32932–32940.
13. Kokoska, R. J., Bebenek, K., Boudsocq, F., Woodgate, R. & Kunkel, T. A. (2002). Low fidelity DNA synthesis by a y family DNA polymerase due to misalignment in the active site. *J. Biol. Chem.* **277**, 19633–19638.
14. Vaisman, A., Ling, H., Woodgate, R. & Yang, W. (2005). Fidelity of Dpo4: effect of metal ions, nucleotide selection and pyrophosphorolysis. *EMBO J.* **24**, 2957–2967.
15. Zang, H., Irimia, A., Choi, J. Y., Angel, K. C., Loukachevitch, L. V., Egli, M. & Guengerich, F. P. (2006). Efficient and high fidelity incorporation of dCTP opposite 7,8-dihydro-8-oxodeoxyguanosine by *Sulfolobus solfataricus* DNA polymerase Dpo4. *J. Biol. Chem.* **281**, 2358–2372.
16. Zang, H., Goodenough, A. K., Choi, J. Y., Irimia, A., Loukachevitch, L. V., Kozekov, I. D. *et al.* (2005). DNA adduct bypass polymerization by *Sulfolobus solfataricus* DNA polymerase Dpo4: analysis and crystal structures of multiple base pair substitution and frameshift products with the adduct 1,N2-ethenoguanine. *J. Biol. Chem.* **280**, 29750–29764.
17. Gruz, P., Shimizu, M., Pisani, F. M., De Felice, M., Kanke, Y. & Nohmi, T. (2003). Processing of DNA lesions by archaeal DNA polymerases from *Sulfolobus solfataricus*. *Nucl. Acids Res.* **31**, 4024–4030.
18. Kokoska, R. J., McCulloch, S. D. & Kunkel, T. A. (2003). The efficiency and specificity of apurinic/apyrimidinic site bypass by human DNA polymerase eta and *Sulfolobus solfataricus* Dpo4. *J. Biol. Chem.* **278**, 50537–50545.
19. Ling, H., Boudsocq, F., Woodgate, R. & Yang, W. (2001). Crystal structure of a Y-family DNA polymerase in action: a mechanism for error-prone and lesion-bypass replication. *Cell*, **107**, 91–102.
20. Ling, H., Boudsocq, F., Plosky, B. S., Woodgate, R. & Yang, W. (2003). Replication of a cis-syn thymine dimer at atomic resolution. *Nature*, **424**, 1083–1087.
21. Ling, H., Sayer, J. M., Plosky, B. S., Yagi, H., Boudsocq, F., Woodgate, R. *et al.* (2004). Crystal structure of a benzo[a]pyrene diol epoxide adduct in a ternary complex with a DNA polymerase. *Proc. Natl Acad. Sci. USA*, **101**, 2265–2269.
22. Ling, H., Boudsocq, F., Woodgate, R. & Yang, W. (2004). Snapshots of replication through an abasic lesion; structural basis for base substitutions and frameshifts. *Mol. Cell.* **13**, 751–762.
23. Trincao, J., Johnson, R. E., Wolfle, W. T., Escalante, C. R., Prakash, S., Prakash, L. & Aggarwal, A. K. (2004). Dpo4 is hindered in extending a G.T mismatch by a reverse wobble. *Nature Struct. Mol. Biol.* **11**, 457–462.
24. Matray, T. J. & Kool, E. T. (1999). A specific partner for abasic damage in DNA. *Nature*, **399**, 704–708.
25. Ren, R. X. F., Chaudhuri, N. C., Paris, P. L., Rumney, S. I. V. & Kool, E. T. (1996). Naphthalene, phenanthrene, and pyrene as DNA base analogs: synthesis, structure, and fluorescence in DNA. *J. Am. Chem. Soc.* **118**, 7671–7678.
26. Batra, V. K., Beard, W. A., Shock, D. D., Krahn, J. M., Pedersen, L. C. & Wilson, S. H. (2006). Magnesium-induced assembly of a complete DNA polymerase catalytic complex. *Structure*, **14**, 757–766.
27. Patel, S. S., Wong, I. & Johnson, K. A. (1991). Pre-steady-state kinetic analysis of processive DNA replication including complete characterization of an exonuclease-deficient mutant. *Biochemistry*, **30**, 511–525.
28. Wong, I., Patel, S. S. & Johnson, K. A. (1991). An induced-fit kinetic mechanism for DNA replication fidelity: direct measurement by single-turnover kinetics. *Biochemistry*, **30**, 526–537.
29. Johnson, A. A. & Johnson, K. A. (2001). Fidelity of nucleotide incorporation by human mitochondrial DNA polymerase. *J. Biol. Chem.* **276**, 38090–38096.
30. Johnson, A. A. & Johnson, K. A. (2001). Exonuclease proofreading by human mitochondrial DNA polymerase. *J. Biol. Chem.* **276**, 38097–38107.
31. Guckian, K. M., Schweitzer, B. A., Ren, R. X.-F., Sheils, C. J., Tahmassebi, D. C. & Kool, E. T. (2000). Factors contributing to aromatic stacking in water: evaluation in the context of DNA. *J. Am. Chem. Soc.* **122**, 2213–2222.
32. Bommarito, S., Peyret, N. & SantaLucia, J., Jr (2000). Thermodynamic parameters for DNA sequences with dangling ends. *Nucl. Acids Res.* **28**, 1929–1934.
33. Doktycz, M. J., Paner, T. M., Amaratunga, M. & Benight, A. S. (1990). Thermodynamic stability of the 5′ dangling-ended DNA hairpins formed from sequences 5′-(XY)2GGATAC(T)4GTATCC-3′, where X,Y = A, T, G, C. *Biopolymers*, **30**, 829–845.
34. Sugimoto, N., Matsumura, A., Hasegawa, K. & Sasaki, M. (1991). Effect of dangling ends on the stability of a DNA double helix. *Nucl. Acids Symp. Ser.* **25**, 51–52.
35. Washington, M. T., Helquist, S. A., Kool, E. T., Prakash, L. & Prakash, S. (2003). Requirement of Watson-Crick hydrogen bonding for DNA synthesis by yeast DNA polymerase eta. *Mol. Cell. Biol.* **23**, 5107–5112.
36. Wolfle, W. T., Washington, M. T., Kool, E. T., Spratt, T. E., Helquist, S. A. *et al.* (2005). Evidence for a Watson-Crick hydrogen bonding requirement in DNA synthesis by human DNA polymerase kappa. *Mol. Cell. Biol.* **25**, 7137–7143.
37. Morales, J. C. & Kool, E. T. (2000). Varied molecular interactions at the active sites of several DNA polymerases: nonpolar nucleoside isosteres as probes. *J. Am. Chem. Soc.* **122**, 1001–1007.
38. Kool, E. T. (2002). Active site tightness and substrate fit in DNA replication. *Annu. Rev. Biochem.* **71**, 191–219.
39. Garcia-Diaz, M., Bebenek, K., Krahn, J. M., Pedersen, L. C. & Kunkel, T. A. (2006). Structural analysis of strand misalignment during DNA synthesis by a human DNA polymerase. *Cell*, **124**, 331–342.
40. Otwinowski, Z. & Minor, W. (1997). Processing of X-ray diffraction data collected in oscillation mode. *Methods Enzymol.* **276**, 307–326.
41. Brunger, A. T., Adams, P. D., Clore, G. M., DeLano,

W. L., Gros, P., Grosse-Kunstleve, R. W. *et al.* (1998). Crystallography and NMR system: a new software suite for macromolecular structure determination. *Acta Crystallog. sect. D*, **54**, 905–921.
42. Jones, T. A., Zou, J. Y. & Cowan, S. W. (1991). Improved methods for building protein models in electron density maps and the location of errors in these models. *Acta Crystallog. sect. A*, **47**, 110–119.
43. Murshudov, G. N., Vagin, A. A., Lebedev, A., Wilson, K. S. & Dodson, E. J. (1999). Efficient anisotropic refinement of macromolecular structures using FFT. *Acta Crystallog. sect. D*, **55**, 247–255.
44. Winn, M. D., Isupov, M. N. & Murshudov, G. N. (2001). Use of TLS parameters to model anisotropic displacements in macromolecular refinement. *Acta Crystallog. sect. D*, **57**, 122–133.

Edited by J. Karn

(Received 9 September 2006; received in revised form 29 September 2006; accepted 2 October 2006)
Available online 7 October 2006